



## ORIGINAL RESEARCH

# Wideband 0.5–50 GHz double-ridged guide horn antenna using coaxial-to-ridge waveguide launcher

 Bennie Jacobs | Johann W. Odendaal  | Johan Joubert 

Department of EEC Engineering, Centre for Electromagnetism, University of Pretoria, Pretoria, South Africa

## Correspondence

 Johann W. Odendaal, Department of Electrical, Electronic and Computer Engineering, Private Bag X20, Hatfield, South Africa.  
Email: [wimpie.odendaal@up.ac.za](mailto:wimpie.odendaal@up.ac.za)

## Funding information

SAAB Grintek Defence

## Abstract

Ever-increasing bandwidth requirements from various industries drive the need for the ever-increasing bandwidth of antennas used for testing. Broadband Double-Ridged Guide Horn (DRGH) antennas are used extensively in antenna measurement and ElectroMagnetic Compatibility/Interference (EMC/I) testing. The current state-of-the-art broadband DRGH antennas reported in the literature for use in measurement applications cover bandwidth ratios as large as 36:1 (0.5–18 GHz). This paper presents the design and realisation of a DRGH antenna with a 100:1 bandwidth ratio (0.5–50 GHz). To achieve such a wide bandwidth, the ridge gap, width and feed were optimised, and a novel coaxial-to-ridge waveguide launcher section based on a typical Vivaldi antenna was developed. Backward radiation was reduced using an absorber-filled cavity. A prototype DRGH antenna was manufactured using additive manufacturing, also referred to as 3D printing. Simulated and measured results obtained in an anechoic chamber are presented.

## KEYWORDS

antennas, antenna testing, broadband antennas, horn antennas, ridge waveguides, ultra wideband antennas

## 1 | INTRODUCTION

Worldwide, various industries have an ever-increasing need for wider bandwidth systems. As an example in the telecommunications industry, the latest technology standard (3GPP TS 38.101–1, release 18) for broadband 5G cellular networks calls for operation in frequency ranges from 410 to 7125 MHz (FR1), 24.25–52.6 GHz (FR2-1) and 52.6–71 GHz (FR2-2) [1]. In the defence industry, frequency range requirements for modern Radar Electronic Support Measures (RESM) systems are from a few hundred MHz to above 40 GHz and for Communication Electronic Support Measures (CESM) from a few kHz up to 9 GHz or more.

Typically, ultra-wideband systems require a number of antennas to cover the wide frequency bands. Although the speed at which measurement instrumentation such as Spectrum Analysers and Vector Network Analysers (VNA) can perform measurements has increased dramatically over the last decade, the testing of these systems can be extremely time-consuming due to the broad frequency range. One of the factors that can

have a large influence on measurement time is the setup and calibration of different source and reference antennas to cover the different frequency bands. Increasing the operational bandwidth of the antennas used for testing can therefore not only save on measurement time but also on the cost of expensive test antennas, if a single source or reference antenna can replace two or more antennas.

Today broadband ridged horn antennas are widely used for antenna and EMC/I measurements, but the origin of horn antennas goes back well over a century. The development of ridged waveguides in the 1950s [2, 3] and its extension to double-ridged horn antennas allowed a rapid expansion of the bandwidth of horn antennas beyond an octave. Initially in the order of 3:1 [4] and subsequently 12:1 [5–8], with the 12:1 bandwidth made possible by further improvements in the ridge profile, coaxial-to-ridged waveguide launcher and sidewalls.

Adaptions of the antennas proposed in Ref. [8] 50 years ago were the de-facto industry standard for more than 3 decades, with especially the 1–18 GHz DRGH (18:1 bandwidth) being used widely. Deficiencies in the radiation pattern above

This is an open access article under the terms of the [Creative Commons Attribution-NonCommercial-NoDerivs](https://creativecommons.org/licenses/by-nc-nd/4.0/) License, which permits use and distribution in any medium, provided the original work is properly cited, the use is non-commercial and no modifications or adaptations are made.

© 2023 The Authors. *IET Microwaves, Antennas & Propagation* published by John Wiley & Sons Ltd on behalf of The Institution of Engineering and Technology.

12 GHz were exposed using ElectroMagnetic (EM) simulations [9–11] and led to renewed interest in the design of these antennas. Initially, the focus was on solving the pattern deterioration problem, which resulted in several improved designs [12–20]. Further work included manufacturing tolerance and sensitivity studies [21, 22], extending the improvements to other frequency bands [23–25], and improvements in performance by investigating the ridge width, ridge profile, launcher cavity, and sidewalls [26–29]. Some of the improvements also resulted in slightly wider bandwidths in the order of 20:1 and 25:1 [17, 19, 24, 27]. In Ref. [30], an 83:1 bandwidth (0.6–50 GHz) DRGH is proposed; however, only simulated results are presented, and a lack of information makes it difficult to thoroughly validate this design. The antenna gain is also presented in very large frequency steps, and it is possible that narrow dips in the gain could have been missed—which usually is an indication of pattern break-up. The widest bandwidth DRGH antenna validated by measured results was presented in Ref. [31], with a design that operates from 0.5 to 18 GHz for a 36:1 bandwidth.

This paper presents the design and realisation (using additive manufacturing) of a single antenna that can be used to measure 0.5–50 GHz antennas and systems as a source antenna in an anechoic chamber, as a gain reference antenna, and for EMC/I testing. A parametric study was performed to identify critical parameters in the design of a 0.5–50 GHz DRGH antenna for a bandwidth ratio of 100:1. To cover such a wide bandwidth, a novel coaxial-to-ridged waveguide launcher section is presented. It was also necessary to reduce the ridge gap and width and use absorbing materials inside the cavity. A prototype DRGH antenna as shown in Figure 1 was manufactured using additive manufacturing and measured in an anechoic chamber.

The electrical design of the 0.5–50 GHz horn is presented in Section 2. The mechanical design and additive



**FIGURE 1** Prototype 0.5–50 GHz DRGH antenna realised using additive manufacturing

manufacturing method to realise a prototype antenna are presented in Section 3. Section 4 shows a comparison between simulated and measured results for the DRGH antenna. In Section 5, the 0.5–50 GHz DRGH antenna is compared to other DRGH antenna designs available in the literature, with concluding remarks in Section 6.

## 2 | ELECTRICAL DESIGN OF A 0.5–50 GHz DRGH ANTENNA

The main goal was to investigate what is needed to extend the bandwidth of the 0.5–18 GHz DRGH [31] up to 50 GHz. A number of these antennas [31] are currently used as a broadband source and reference antennas for measuring other antennas and antenna systems in anechoic chambers. It was required that the bandwidth extension should not degrade the performance below 18 GHz. Similar performance to that achieved by the authors in Ref. [31] above 18 GHz was desired in the mm-wave band, VSWR typically less than 2:1 and at most 2.5:1, and a nominal boresight gain of 14 dBi. To ensure magnitude and phase uniformity in the quiet zone of the anechoic chamber, the main beam should not have any pattern breakup, and side and back lobe levels should be similar to [31]. As the focus is on anechoic chamber use and not high-power EMI/EMC testing, it was not required that the antenna should be able to handle much more than 1 W CW power.

The 0.5–50 GHz horn antenna is based on the 0.5–18 GHz horn presented in Ref. [31], and simulations were performed using an improved FEKO [32] EM model. For better accuracy in the mm-wave band, the simplified FEKO EM model of [31] was improved by replacing the Perfect Electrical Conducting (PEC) triangles with metallic triangles having the conductivity of gold ( $4.098 \times 10^7$  S/m, feed), aluminium ( $3.816 \times 10^7$  S/m, mechanical parts), and copper ( $5.813 \times 10^7$  S/m, sidewall strips). A surface roughness equivalent to typical machining tolerances, Root Mean Square (RMS) of  $22 \times 10^{-6}$  m, was applied to all mechanical triangles on machined parts, and the sidewalls were modelled using a thin dielectric sheet approximation instead of only modelling the grids and ignoring the FR4 Printed Circuit Board (PCB)-based material. This change is especially important for frequencies above 20 GHz where the dielectric in the sidewalls has a large impact.

The general triangle edge length was set to  $\lambda/3$  (the minimum allowed in FEKO) at 50 GHz, but with smaller local mesh sizes used in known sensitive regions, viz. the feed structure. The final model consisted of 98 038 triangles. In the mm-wave band, simulations were performed in 500 MHz steps from 18 to 50 GHz. For the basic model, these simulations showed deep dips in gain above 20 GHz caused by pattern deterioration and impedance mismatch above 29 GHz. The reason for the gain dips and pattern deterioration has been widely accepted as the existence of higher-order modes, but it was found that the cause is also related to reflections and diffraction from the cavity and sidewalls.

A parametric study was performed to identify the effect and critical parameters in the coaxial feed and cavity section, ridge

profiles, and sidewalls of the DRGH antenna. The effect of the different parts was investigated in isolation, that is, the basic 0.5–18 GHz model as described above was used as a starting point in each section, and changes were only performed on the specific parts as indicated in the respective sections. All the proposed design changes from Sections 2.1–2.4 were then combined and implemented together in Section 2.5.

## 2.1 | Coaxial feed section

Deep dips in gain and/or large VSWR peaks can be caused by modes due to the incorrect connector choice and/or modes in the coaxial impedance transformer. Therefore, the connector was changed to a 2.4 mm connector that would allow mode-free operation up to 50 GHz. Using a 2.4 mm connector allows a higher frequency of operation, but with a reduced power handling capability, in the order of 114 W CW at 1 GHz decreasing to 16 W CW at 50 GHz [33]. The final connector chosen was the Southwest Microwave model 1412-04SF 2.40 Jack (F) 0.375" square flange connector. This connector allows the use of a feed pin with a diameter of 0.51 mm, and for the ease of manufacturing, the outer conductor of the coaxial impedance transformer was tapered and not the feed pin forming the inner conductor since manufacturing a taper on such a small feed pin size will be challenging. The outer conductor was designed to taper from a 1.2 mm diameter at the connector to 0.9 mm at the ridge for an impedance taper of 50–34  $\Omega$  [31]. To reduce manufacturing complexity, the final taper length was restricted to approximately half of the E-plane cavity dimension.

## 2.2 | Design of the ridges

The effect of several ridge parameters was investigated by performing a parametric study with an EM model that excluded the sidewalls and cavity. For faster simulations, the model was simplified by removing the impedance transformer and keeping only 1 mm of the coaxial feedline inside the ridge,

allowing the implementation of the FEKO waveguide feed model (see Figure 2).

The parametric study on the dimensions of the ridge gap and width was performed using the basic 0.5–18 GHz FEKO model with a scale factor less than 1 to reduce the ridge dimensions since it is expected that for a higher frequency of operation, the ridge parameters will be smaller. The parameters were first scaled independently starting with the ridge gap. Figures 3 and 4 show the VSWR and boresight gain for a scale factor from 1 to 0.5 in 0.05 steps for the ridge gap. As the gap size decreases, the VSWR degrades across the band, indicating a change in ridge impedance, with significant increases in VSWR observed around 800 MHz and above 30 GHz. The gain stays mostly the same, except the dip around 32 GHz becoming deeper with the reduced gap size.

Next, the ridge width was investigated—the ridge width taper angle was kept the same, only the width at the start of the ridge was changed. Note that the feed pin and feed outer conductor size are related to the ridge width as the ridge width must be larger than the outer conductor by some margin to accommodate the feed. For practical implementation, the ridge width should at least be 1 mm larger than the outer conductor diameter. A feed pin diameter of 0.51 mm and an outer conductor diameter of 0.9 mm were used, for an impedance of 34  $\Omega$  at the feed point. Figures 5 and 6 show the VSWR and boresight gain for a scale factor from 1 to 0.5 in 0.05 steps for the ridge starting width. Reducing the ridge starting width significantly improved the VSWR and gain above 24 GHz, although between 2 and 24 GHz, the VSWR did degrade slightly—indicating that the ridge impedance over this frequency range do vary slightly.

In the next step, the ridge gap, starting ridge width, and feed parameters (feed pin and outer conductor diameter) were all scaled together, starting with the model used in the ridge gap investigation and using a scale factor from 1 to 0.5 in 0.05 steps. Figures 7 and 8 show a significant improvement in the VSWR and gain above 24 GHz. Interestingly, the VSWR below 24 GHz showed nearly no effect which indicates that scaling the ridge width and ridge gap together, that is, keeping the ratio of ridge gap to width constant, keeps the characteristic ridge

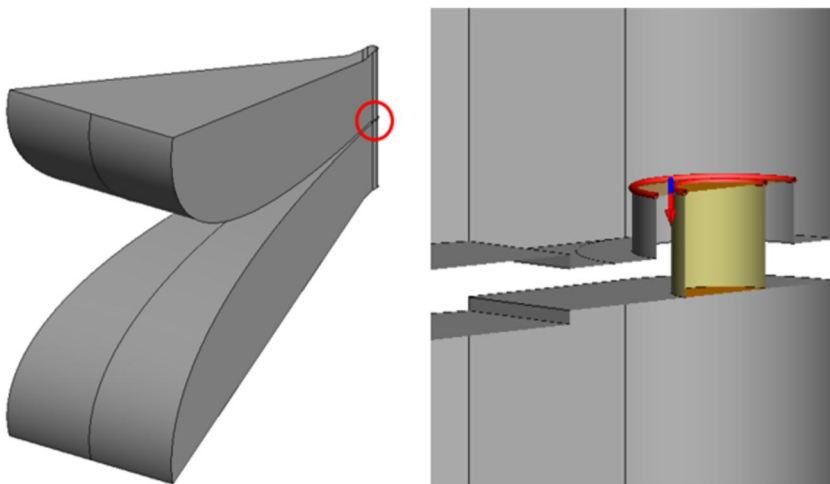


**FIGURE 2** Simplified FEKO model for the ridge gap and width investigations.

**FIGURE 3** VSWR performance for different ridge gap dimensions.

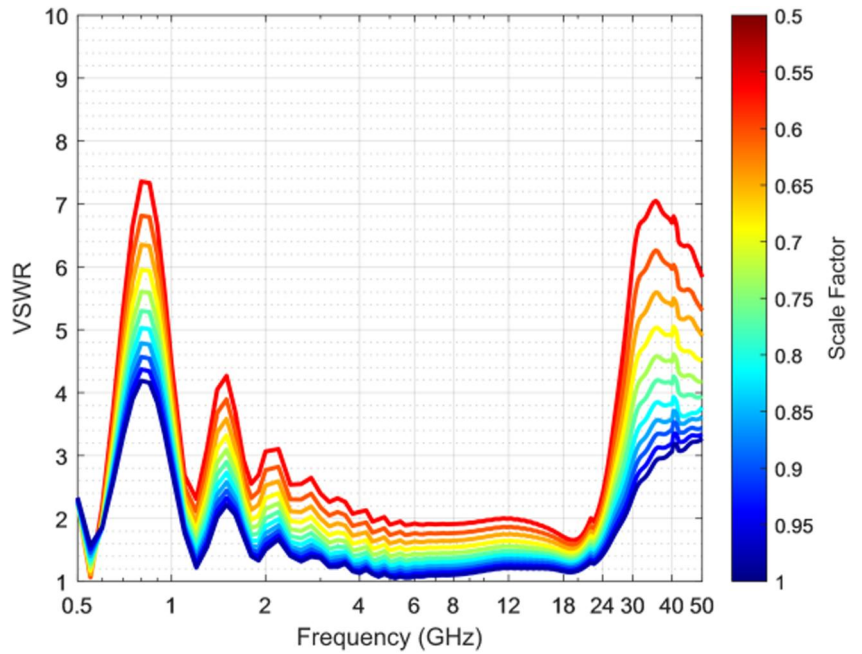
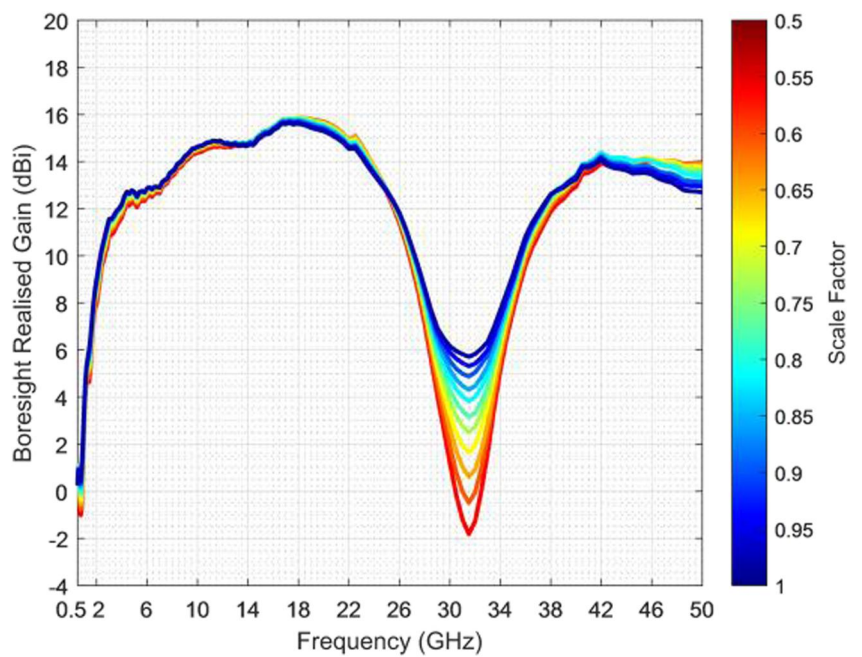


**FIGURE 4** Boresight gain performance for different ridge gap dimensions.



impedance constant over most of the frequency range. It was found that a scale factor of 0.5 or less resulted in a 3D radiation pattern with a well-formed main beam over the full frequency range.

In summary, Figures 3 and 4 show that the gain dip at 32 GHz becomes deeper and the VSWR, especially below 2 GHz and above 24 GHz, degrades if the ridge gap is reduced and the ridge width is kept constant. Figures 5 and 6 show that reducing the ridge width in isolation removes the dip in the gain at 32 GHz and improves the VSWR above 24 GHz, but the VSWR between 2 and 24 GHz increases. Figures 7 and 8 show that by decreasing both the ridge gap and width, the gain

performance improves, while the VSWR below 2 GHz and above 24 GHz remains virtually the same, with a significant improvement of the VSWR performance between 2 and 24 GHz.

Based on the ridge investigation, the final chosen values for the ridge parameters are given in Table 1. The coordinate system is defined in Figure 9 with the *Y*-axis going into the page, that is, a right-hand coordinate system. Note that in Ref. [31], the ridge gap had a step, going from 0.7 mm at the feed to 1.1 mm at the launcher interface. For the ease of manufacture, it was decided to remove this step for the new design. Similar to [31], a short straight ridge section was used between the feed

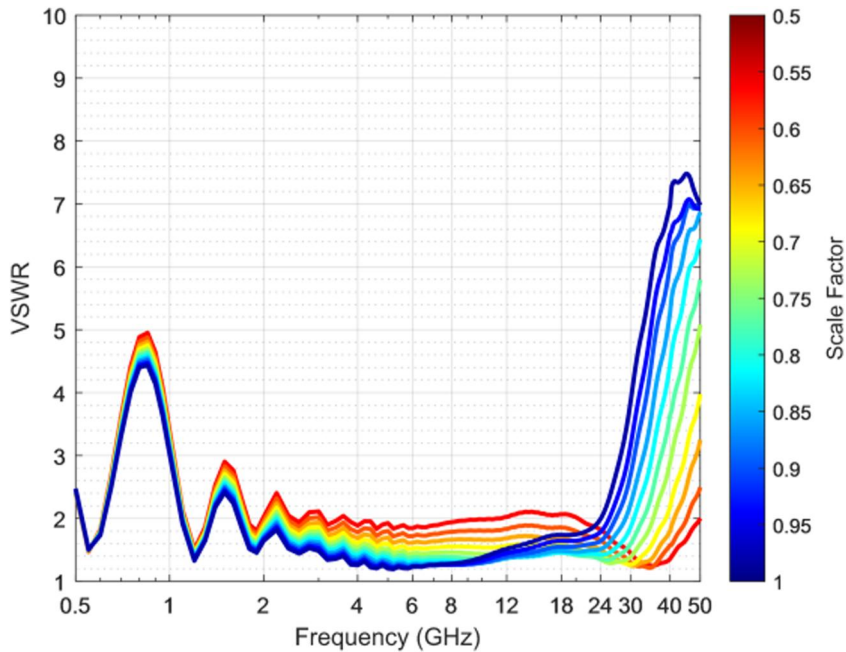


**FIGURE 5** VSWR performance for different ridge width dimensions.

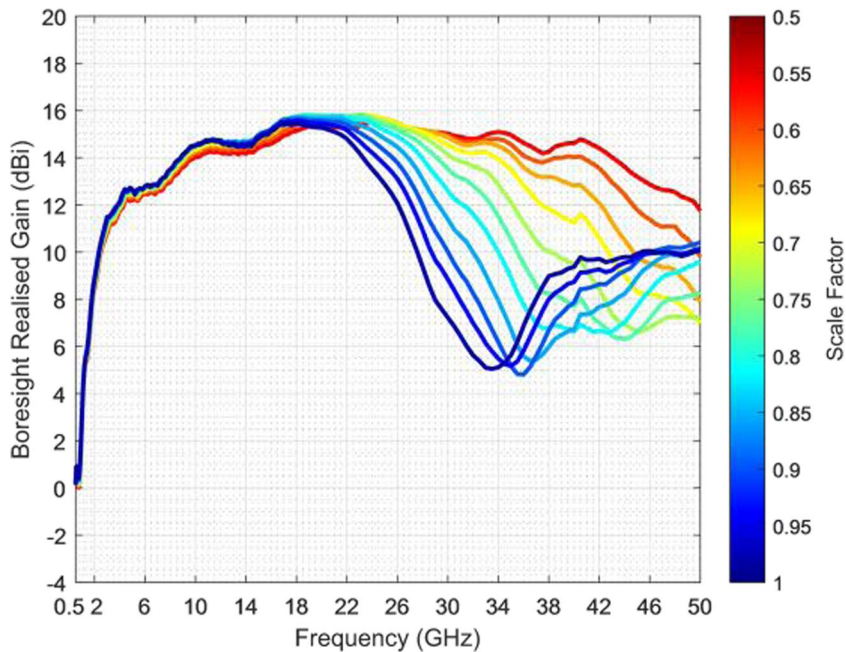


**FIGURE 6** Boresight gain performance for different ridge width dimensions.

point (at  $X = 0$  mm) and the start of the Bezier curve, but the length of this straight section was reduced slightly.

### 2.3 | Design of the flared waveguide and sidewall section

The effect of the sidewalls was evaluated by removing the dielectric E-plane sides and grids; and finally both the E- and H-plane sides from the 0.5–18 GHz antenna. It was observed that removing the dielectric substrate of the E-plane sides had virtually no effect on the VSWR but influenced the gain above

20 GHz. Removing the E-plane grid had very little further effect on the mm-wave gain but resulted in degraded VSWR performance below 2 GHz which resulted in a lower realised gain below 2 GHz. The removal of the H-plane sides degraded the VSWR and gain below 2 GHz further and slightly effected the gain in the mm-wave band.

At first glance, the impact of the dielectric substrate of the sidewalls on the gain above 20 GHz seemed deceptively small, just a slight frequency shift of peaks and dips in the gain. However, a more thorough analysis of the 3D radiation patterns revealed that the substrate does have a significant impact on the patterns and causes pattern deterioration. For the upper

**FIGURE 7** VSWR performance for different ridge gap and width dimensions.

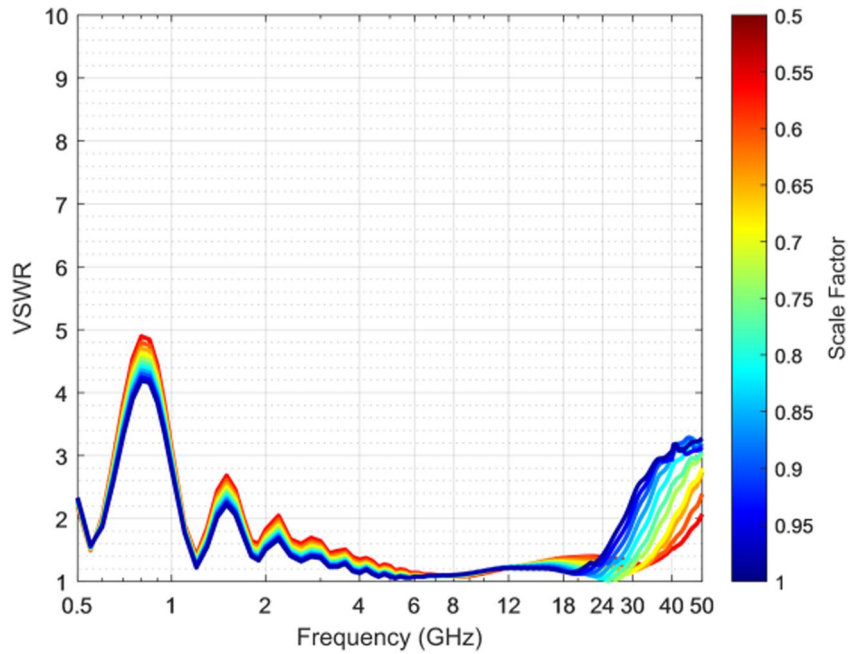
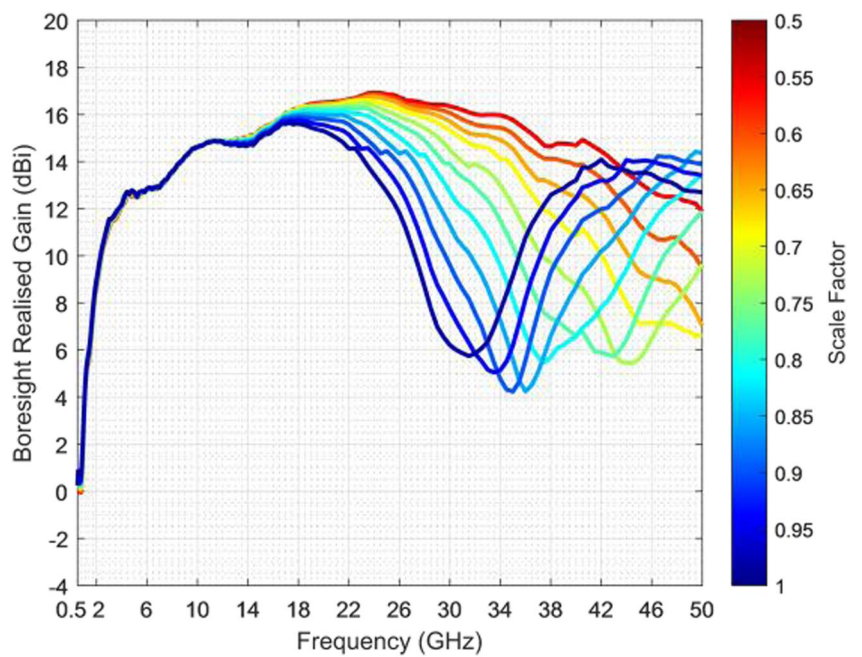


**FIGURE 8** Boresight gain performance for different ridge gap and width dimensions.



frequencies, the point at which the guided wave becomes a radiating wave will occur much deeper into the horn which can result in reflections from sidewalls that will cause pattern deterioration.

The final E-plane sidewall electrical design consists of thin grids without any dielectric supports with a strip width of 1 mm and a strip gap of 60 mm ( $\lambda/10$  at 0.5 GHz) [31]. The E- and H-plane aperture dimensions were kept the same as in Ref. [31], that is,  $264 \times 152$  mm and the same for the other end of the flared waveguide at the launcher interface, that is,  $80 \times 60$  mm. The flared waveguide axial length was increased

slightly (194.55 mm) so that the starting point of the flare would align with that of the ridge Bezier curve.

## 2.4 | Design of the launcher and cavity

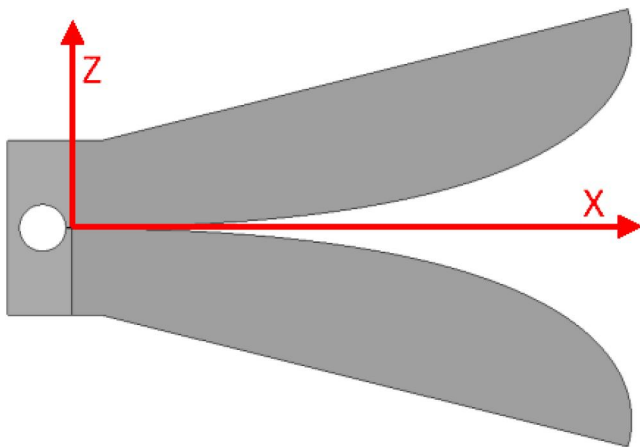
The effect of the cavity was investigated by first removing the front part of the cavity and then also with the full cavity removed. It was observed that removing the first section of the cavity had very little effect on either the VSWR or gain, but removing the full cavity significantly changed the VSWR

**TABLE 1** Ridge design parameters (in mm).

Parameter	Value
Ridge gap at start ( $Z$ -axis)	0.4 <sup>a</sup>
Ridge width at start ( $Y$ -axis)	2.5 <sup>a</sup>
Ridge width at end ( $Y$ -axis)	77.1
Bezier P0 (start point)	( $X: 1.25, Z: \pm 0.2$ ) <sup>b</sup>
Bezier P1 (start tangent point)	( $X: 225.32, Z: \pm 0.2$ ) <sup>b</sup>
Bezier P2 (end tangent point)	( $X: 192.99, Z: \pm 75.99$ ) <sup>b</sup>
Bezier P3 (end point)	( $X: 193, Z: \pm 76$ ) <sup>b</sup>

<sup>a</sup>Approximate scale factor of 0.5 (Figures 7 and 8).

<sup>b</sup>Note that the  $\pm$  values are for the top and bottom ridges, respectively.

**FIGURE 9** Ridges with the Vivaldi feeding structure/circular cavity.

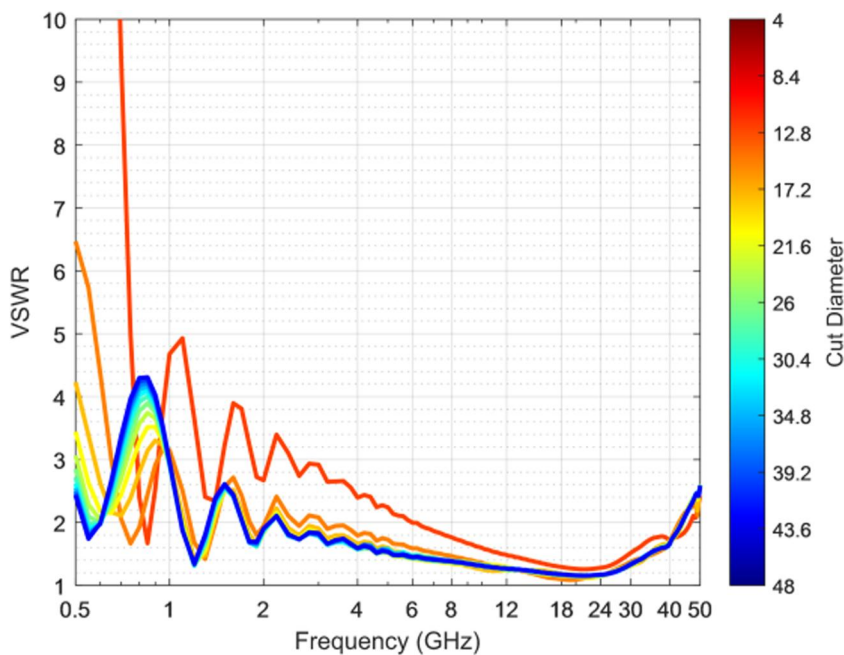
between 0.5–2 GHz and the gain above 6 GHz, especially between 20 and 34 GHz.

The impact of the cavity on the patterns above 20 GHz is significant. A review of all the 3D patterns over the full 0.5–50 GHz band shows that for the case of no cavity, a useable main beam is maintained over the full frequency range. There is however a significant back lobe, the worst case being only 5 dB below the main lobe. It was also found that above 20 GHz, side lobes start to appear that increase to around 10 dB below the main lobe. It is believed that the interaction between these side lobes and back lobes with the cavity and sidewalls causes additional pattern deterioration.

For the physical implementation of the horn, the antenna needs a structure to which the top and bottom ridges can be connected. This function is performed by the cavity. The cavity also ensures that the energy entering the horn through the connector and down the coaxial impedance transformer is guided along the ridges in the boresight direction. Effectively, the cavity or coaxial-to-ridged waveguide launcher acts as a balun. Vivaldi antennas can be considered a 2D implementation of the 3D ridges in a DRGH. A structure similar to the balun of a conventional Vivaldi antenna, shown in Figure 9, was thus investigated.

Parametric studies were performed to determine the diameter of the slot line open or circular cavity as well as the distance between the circular cavity and coaxial feedline. These studies used the final ridge design and model as presented in Section 2.2.

Figures 10–13 show the results for these parametric sweeps. It was found that decreasing the circular cavity diameter degrades the low-frequency performance. Increasing the distance between the circular cavity and the feedline deteriorates the high-frequency performance. The optimal value is a cavity diameter of 16 mm, positioned as close as possible to the feedline.

**FIGURE 10** VSWR performance for different circular cavity dimensions.

**FIGURE 11** Boresight gain performance for different circular cavity dimensions.

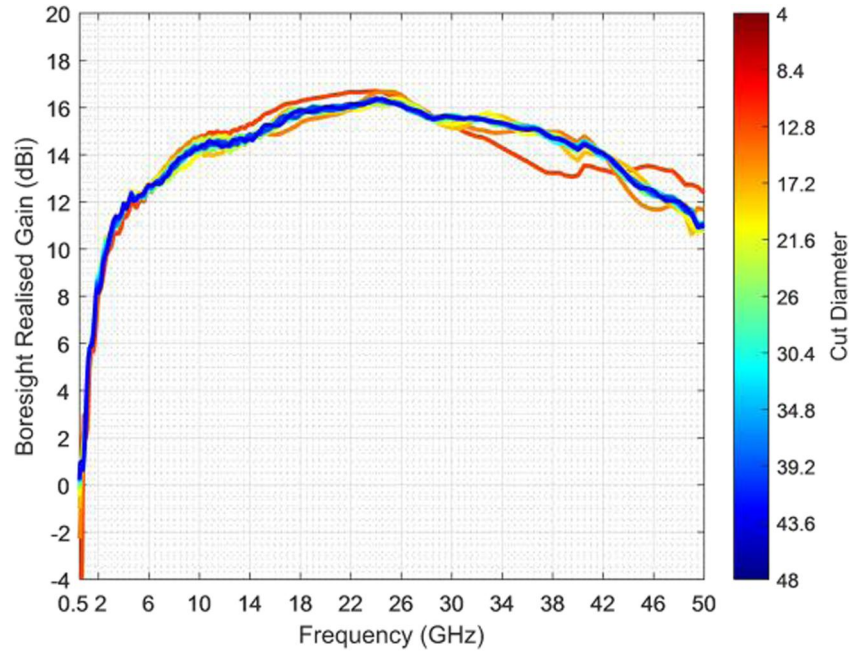
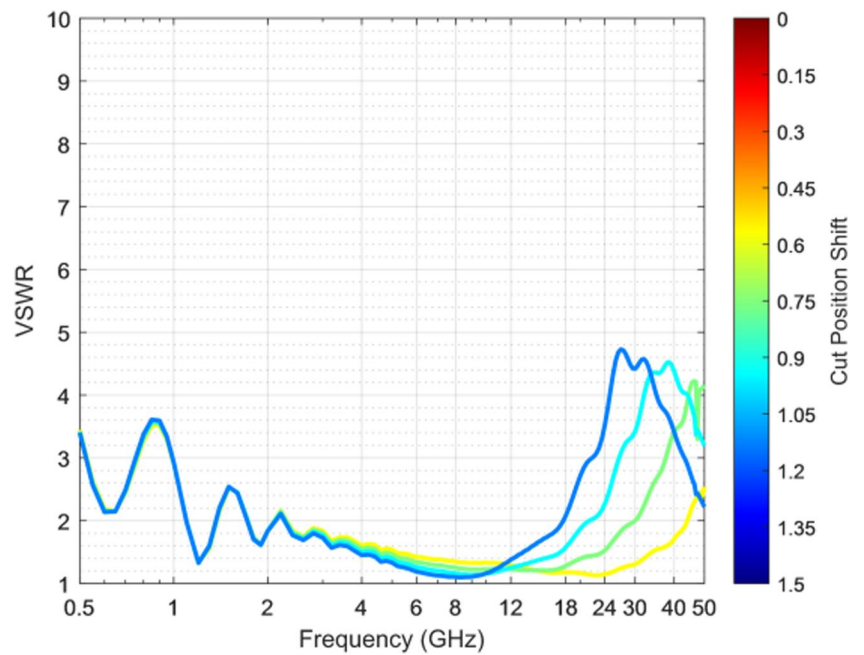


**FIGURE 12** VSWR performance for different distances between circular cavity (16 mm diameter) and feed point.



This coaxial-to-ridged waveguide launcher improved the impedance performance, but there was still significant radiation backwards and to the sides. Since the 2.4 mm connector already limits the power handling capability of the DRGH, an absorber-filled cavity similar to that used on spiral antennas [34] to suppress the backward radiation was added to the Vivaldi structure, Figure 14. The effect of adding the absorber in the cavity on the power handling capability of the antenna is investigated further in Section 4.

The box for the absorber-filled cavity has the same width and height as the waveguide to the launcher interface,

that is,  $80 \times 60$  mm. The depth of the cavity was chosen as 31 mm so that the top of a 0.75-inch absorber would nominally coincide with the centre of the circular cavity. The absorber could either be of the foam type, for example, Eccosorb AN-74 or honeycomb which would be better for higher power handling.

Similar to [34], a honeycomb absorber with hexagonal cells was used in the simulation model. The honeycomb structure was created using a dielectric material coated with a resistive material and graded with an increase towards the bottom of the cavity to maximise absorption.



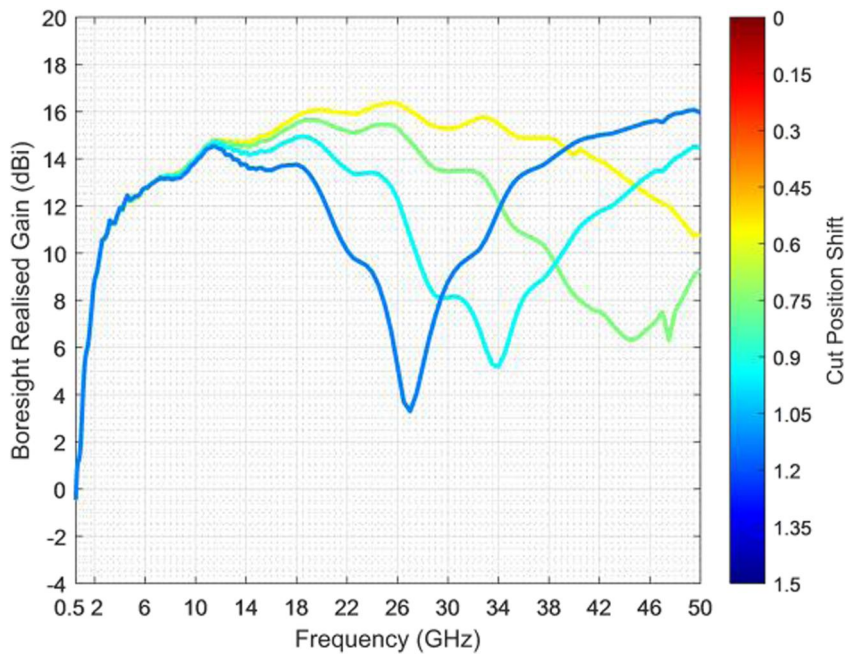


**FIGURE 13** Bore-sight gain performance for different distances between circular cavity (16 mm diameter) and feed point.

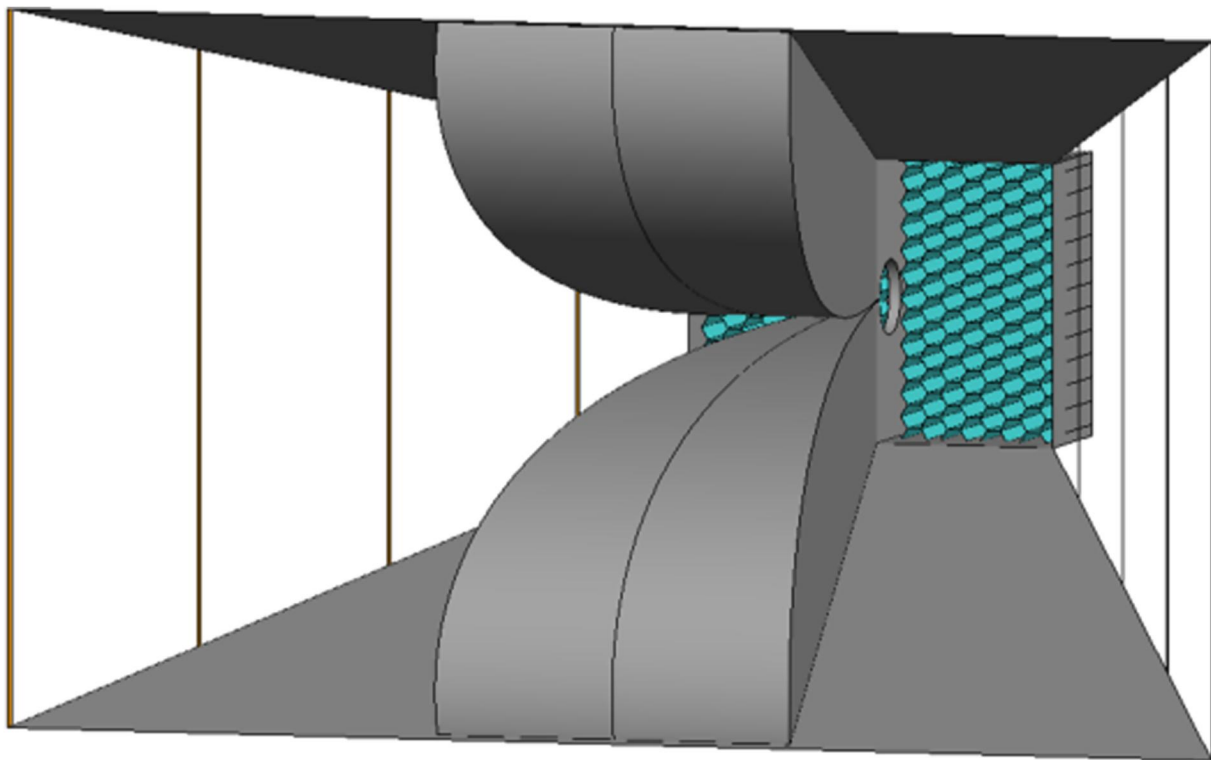


**FIGURE 14** FEKO model showing honeycomb absorber-filled cavity.

## 2.5 | Numerical design optimization

A numerical model was implemented in FEKO based on the best overall performance observed in Sections 2.1–2.4, shown in Figure 15 (top left). The VSWR and bore-sight gain performance for this initial DRGH antenna are shown in Figures 16 and 17, respectively. Further optimisation was

performed, and it was found that adding a smaller sub-ridge inside the main ridge, as well as applying three different main ridge width tapers improved the high-frequency gain and low-frequency VSWR performance.

The implementation of the sub-ridge and different main ridge width tapers are shown in Figure 15 (top right, bottom left, and bottom right). The width of the sub-ridge is 6.5 mm.

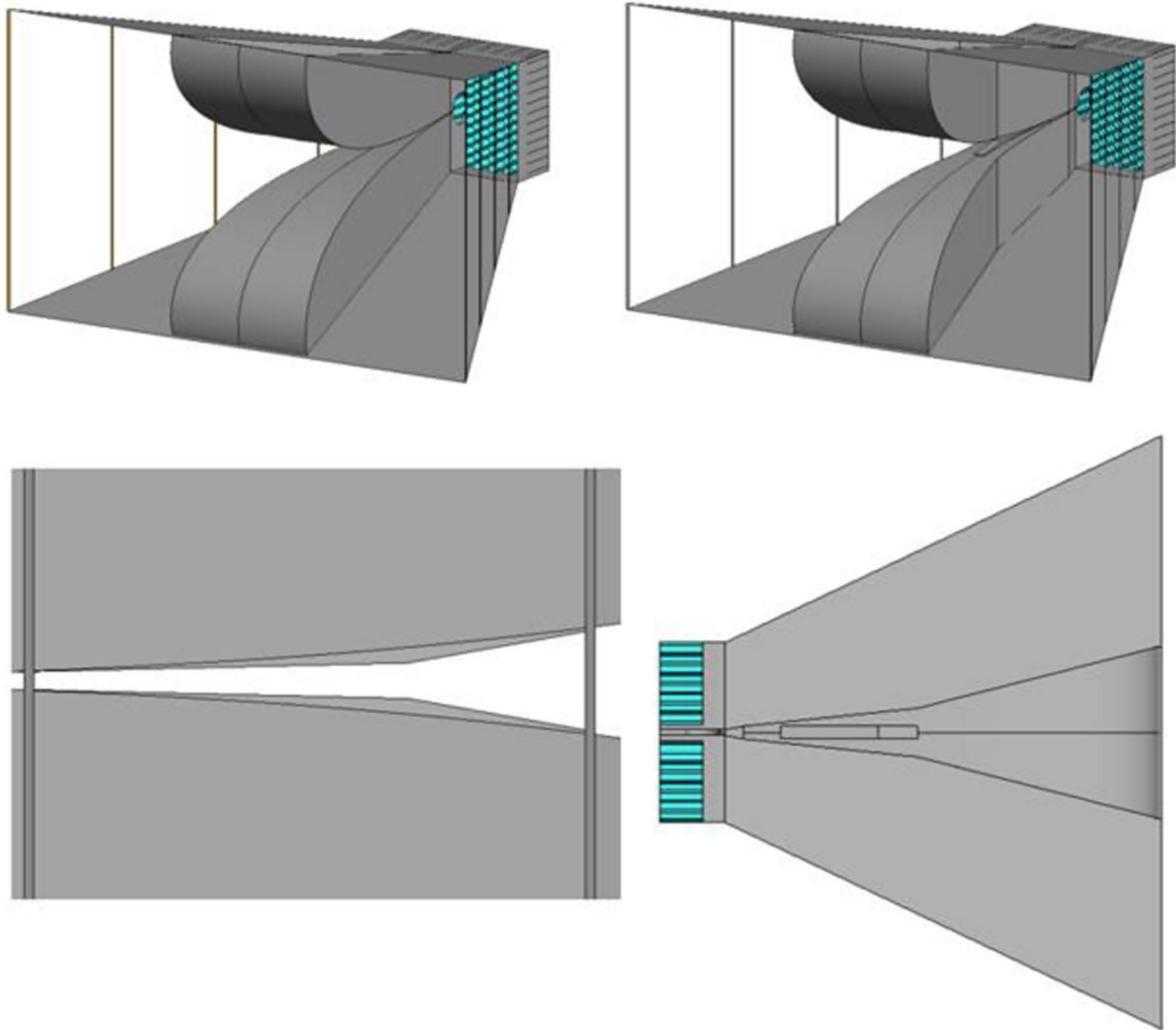


**FIGURE 15** FEKO model for initial (top left) and optimised (top right) DRGH antenna with a side view of sub-ridge (bottom left) and cut view showing the sub-ridge and stepped tapers of the main ridge (bottom right).

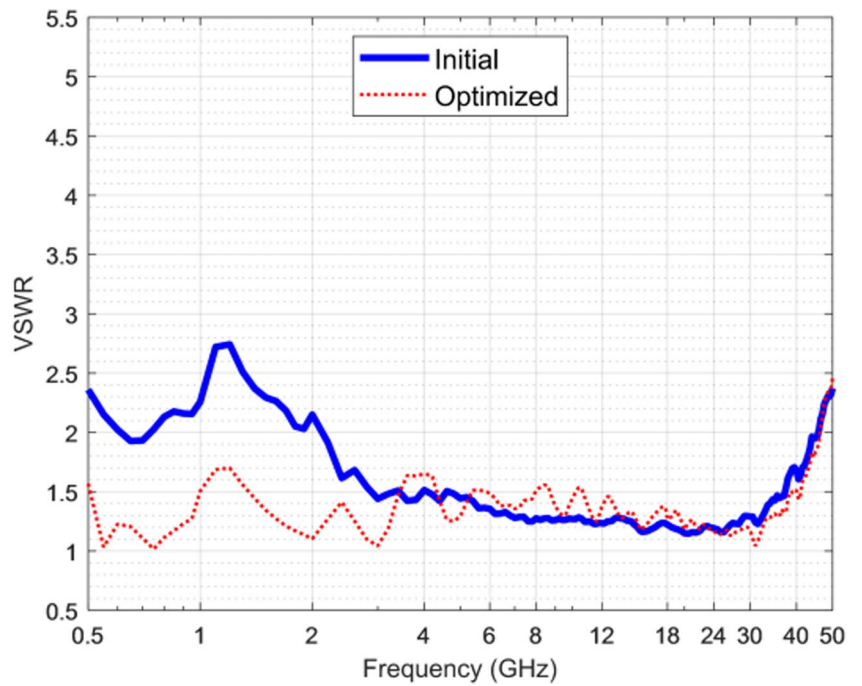


**FIGURE 16** Simulated VSWR for the initial and numerically optimised antenna.

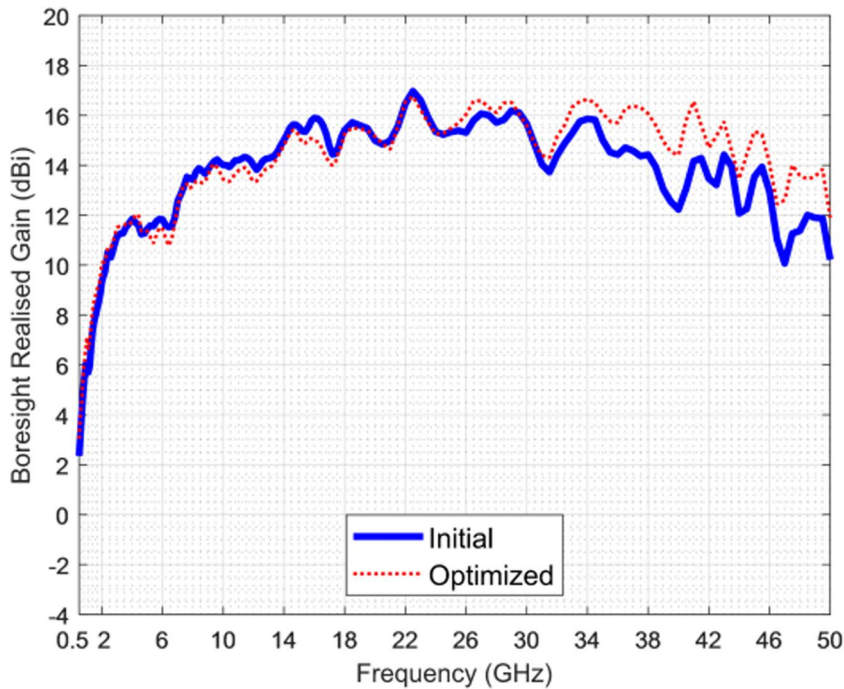


**FIGURE 17** Simulated gain for the initial and numerically optimised antenna.

It starts where the main ridge gap is 1.45 mm. The first section of the sub-ridge is a linear taper at an angle of  $1.3^\circ$  with the horn axis. The second section of the sub-ridge starts where the sub-ridge gap is 3.43 mm, and it also has a linear taper, but at an angle of  $11^\circ$  with the horn axis. The first section of the main ridge is a linear taper at an angle of  $11^\circ$  with the horn axis until the ridge width is 5.61 mm. The second section of the main ridge also has a linear taper, but at an angle of  $5.88^\circ$  until the ridge width is 21.61 mm. The final section of the main ridge has a taper angle of  $14.26^\circ$ .

Figure 16 shows the improved simulated VSWR performance of the optimised design, and Figure 17 shows the improved simulated boresight gain performance.

### 3 | MECHANICAL DESIGN AND IMPLEMENTATION OF THE 0.5–50 GHz DRGH ANTENNA

Most parts of the design were manufactured using additive manufacturing which is a cost-effective way of performing rapid prototype development. The parts not manufactured using additive manufacturing were the 2.4 mm Southwest Microwave connector, the feed pin consisting of a 0.5 mm brass rod, and various Stainless Steel (SS) 316 fasteners and helicoils.

As a starting point, the optimised EM model was given practical thicknesses in FEKO. The E-plane sidewall grid strip width was increased to 3 mm since 1 mm turned out not to be sturdy enough. The model was split into various parts, that is, the ridges, E- and H-plane sidewalls, cavity, and feed section. Details were also added to the various parts, for example, holes for fasteners. The design of the different parts was performed

keeping in mind practical considerations for additive manufacture, such as the size of the parts, alignment on the print bed, support requirements etc. Figure 18 shows the final mechanical design of the antenna.

The STL files were exported from FEKO and imported into the slicer software used by the various printers utilised. Here, details such as layer height, wall thicknesses, fill factor etc., were set up as required. Apart from the feed section, all of the parts were printed in plastic and metallized using a silver conductive spray (842AR from MG Chemicals). The E-plane grids were printed on a VSHAPER in PC-ABS and coated with a silver conductive spray (842AR). The H-plane flares, ridges, and cavity were printed on a Markforged Mark Two in Onyx and coated with a silver conductive spray. The feed section was printed on an EOS M290 in SS316.

The various parts were assembled using fasteners and helicoils inserted into the holes of the printed parts. Silver conductive epoxy was used to glue the ridges to the feed section, and the feed pin was soldered onto the bottom ridge after etching the solder point. The absorber was cut to size and glued into the cavity with attention given to the orientation, that is, ensuring the side least loaded was nearest to the feed point.

The initial measured VSWR result was very poor, and it was determined that the printing tolerances inside the feed section, specifically the coaxial impedance taper, were not good enough. There were obstructions inside the hole that caused the feed pin to short-circuit. To solve this problem, the hole was drilled to a constant diameter of 1.2 mm.

Several experiments were conducted, and it was found that the remaining ripple is due to weak reflections from the cavity edges not covered by the absorber as well as the thin sidewall strips. A foam absorber was placed on the uncovered cavity

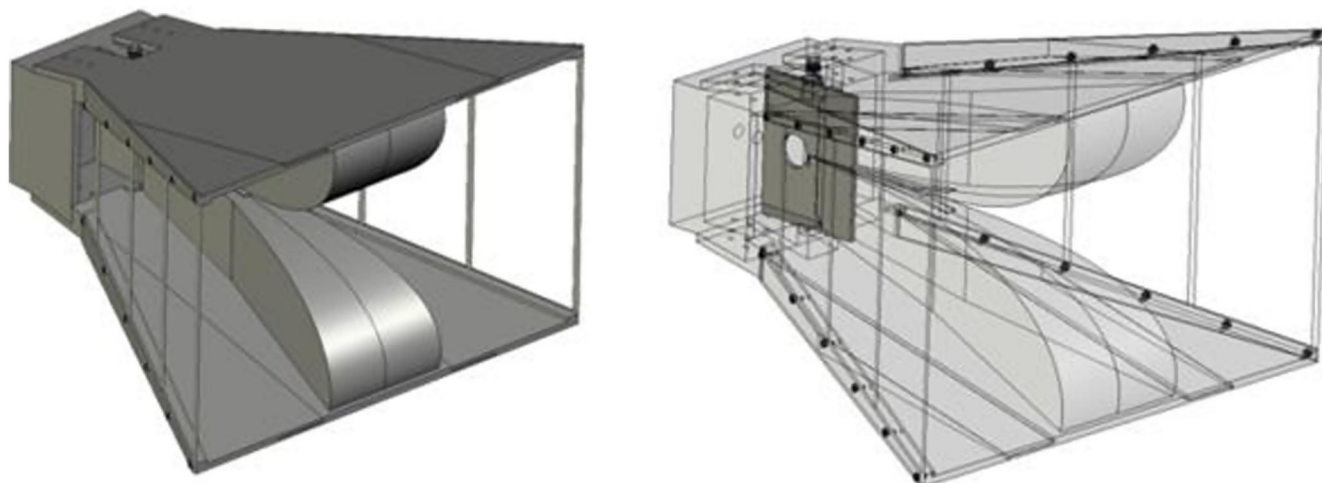


**FIGURE 18** Mechanical design of the horn antenna.

**TABLE 2** Final dimensions of new 0.5–50 GHz DRGH.

Description	Dimension (mm)
<i>H</i> -plane launcher width	80
<i>E</i> -plane launcher width	60
<i>H</i> -plane aperture width	264
<i>E</i> -plane aperture width	152
Feed point to back wall	28.15
Launcher aperture to back wall	31
Flared waveguide axial length	194.55
Feed pin length	35
Feed pin diameter	0.9
Feed outer conductor diameter	1.2
Sidewall strip width	3
Sidewall grid gap	60

edges, and the grid sidewall strips were painted using a carbon conductive paint (Yshield NSF34). These changes did slightly improve the VSWR, gain, and pattern ripple. A photo of the final prototype is shown in Figure 1, and the measured results are presented in the next section. Apart from the final ridge dimensions that are presented in Table 1 and Section 2.5, a summary of the final dimensions of the 0.5–50 GHz DRGH is given in Table 2.

## 4 | SIMULATED AND MEASURED RESULTS

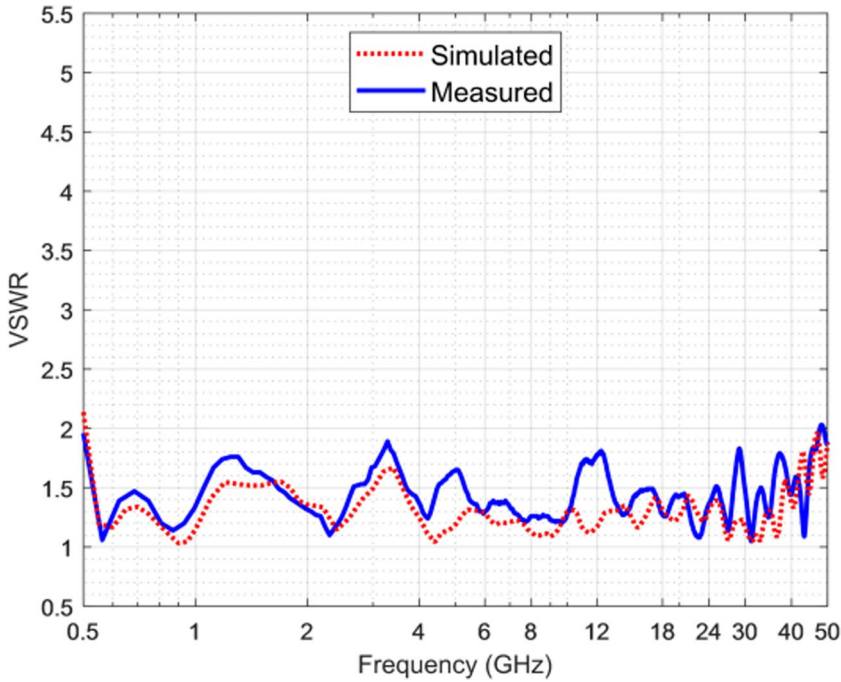
The performance of the prototype antenna was measured in an anechoic chamber using a VNA. To take the mechanical design optimisation into account, and improve the comparison between measured and simulated data, the conductivities of various sections of the simulation model were updated with the

properties of the materials used in the prototype, that is, conductive paint, SS316 for the feed, and brass for the feed pin. The actual thicknesses of the final parts were added to the model. The accuracy of the feed model was improved by adding a numerical model for the 2.4 mm connector and changing the feed outer conductor to a constant 1.2 mm diameter, required due to manufacturing tolerances. The foam absorber was added on the cavity edges and carbon paint on the sidewall strips.

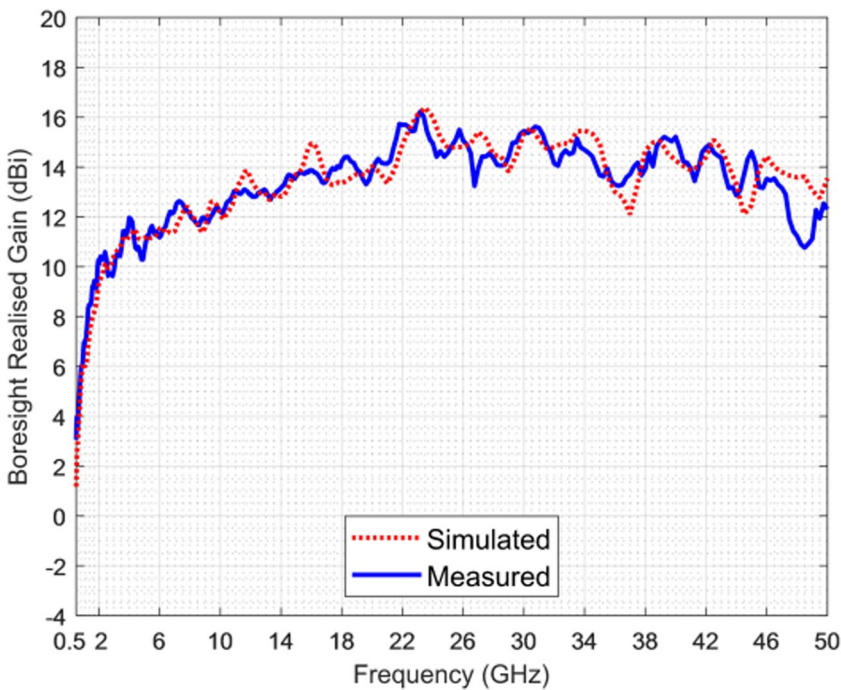
The comparison between measured and simulated VSWR is shown in Figure 19. The maximum measured VSWR is 2.03:1. The deviations between measured and simulated results can be attributed to manufacturing tolerances, especially since printed silver-plated parts were used for which the manufacturing tolerances are significantly worse when compared to machined parts. Figure 20 shows a good comparison between the measured and simulated gain. The gain does have some ripples due to ripples in the main beam pattern, but no pattern breakup was observed in either the measured or the simulated results. Several measured *E*- and *H*-plane radiation patterns are shown in Figure 21.

Figure 22 shows that the total antenna efficiency decreases from a maximum of 0.84 at 2.2 GHz to a minimum of 0.35 at 50 GHz. The side and back lobe levels are shown in Figure 23. As is typical of DRGH antennas, the *E*-plane side lobe levels are very good, typically above 20 dB from 6 GHz, while in contrast, the *H*-plane side lobes reduce from around 15 dB at 18 GHz to a minimum of 7 dB at 48 GHz. The worst-case back lobe is around 3.5 dB at 0.5 GHz and then rapidly improves to 15 dB at 2 GHz and up to 30 dB at 50 GHz. When used as a source antenna in an anechoic chamber, the back lobe can be further reduced by placing a suitable absorber, for example, Eccosorb AN-79, behind the antenna.

The phase centre of the antenna was calculated using the simulation model and is shown in Figure 24. The position of the phase centre varies as a function of frequency and is also different for the *E*- and *H*-plane patterns. The average phase



**FIGURE 19** Comparison between simulated and measured VSWR of the final prototype DRGH.



**FIGURE 20** Comparison between simulated and measured boresight gain of the final prototype DRGH antenna.

centre (mean between the E- and H-plane phase centres) moves from the aperture of the antenna at 0.5 GHz in the direction towards the feed point of the DRGH to a nominal value of 120–140 mm inside the aperture at the high-frequency end.

To investigate whether the power handling capability of the antenna would be constrained by the 2.4 mm connector or the honeycomb absorber, the power density inside the absorber was calculated when the antenna source input power was set to the maximum 2.4 mm power handling [33]. The

results are shown in Figure 25. The maximum power density inside the absorber was found to be less than  $1.1 \text{ kW/m}^2$ , which is well within the claimed power handling of a honeycomb absorber, for example, between  $3 \text{ kW/m}^2$  ( $2 \text{ W/inch}^2$ ) and  $15 \text{ kW/m}^2$  ( $10 \text{ W/inch}^2$ ) [35–39]. This antenna would thus be suitable for use in applications where the required power handling does not exceed the maximum power handling of a 2.4 mm connector, that is, 114 W CW at 1 GHz down to 16 W CW at 50 GHz.

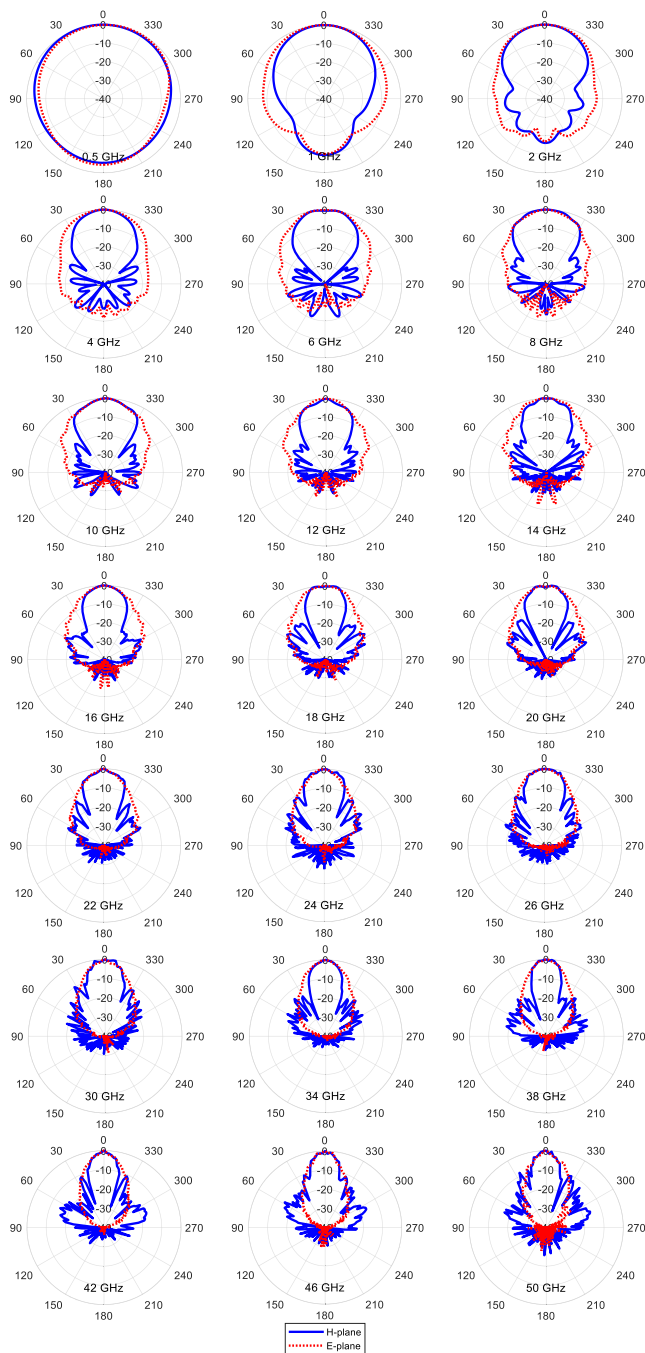


**FIGURE 21** Normalised E- and H-plane measured radiation patterns of the final prototype DRGH antenna.

## 5 | DRGH BANDWIDTH AND DESIGN COMPARISON

As mentioned in the introduction, several DRGH designs achieve bandwidth ratios larger than 18:1. Table 3 shows a comparison between the current DRGH antenna design and other designs available in the literature.

The 20:1 bandwidth design of [24] is significantly smaller than the proposed design presented in this paper. It does not have any E-plane sidewalls and includes a dielectric lens. It has

a standard empty rectangular box coaxial-to-ridged waveguide launcher. The ridge design is also relatively standard with a constant ridge width and exponential ridge profile. Unlike conventional designs, it has slots cut into the ridges.

Patent [16] gives detail design information for a 22.5:1 bandwidth design. Results for this design are available in the datasheet [17]. This antenna has full metal sidewalls with trapezoidal cuts through which the ridges (called fins in Ref. [16]) protrude. The ridges have a constant width with a unique profile described in detail in Ref. [16]. The antenna is significantly larger than the proposed DRGH. A small piece of carbon foam absorber is placed inside a cavity pocket formed by the flares of the coaxial-to-ridged waveguide launcher behind the feed/ridges as opposed to the honeycomb absorber-filled box of this work (which is more akin to the implementation of cavity-backed spiral antennas [34]). The foam is directly behind the feed point, whereas in the proposed DRGH, the Vivaldi connecting structure is behind the feed point.

The design of [27] has adjustable metallic sidewalls compared to fixed metallic sidewalls with carbon loading in the proposed design. It is, however, unclear whether a continuous adjustment of the sidewalls is required to realise the full operational bandwidth of this antenna. The coaxial-to-ridged waveguide launcher is mostly similar to traditional 1–18 GHz designs with flares [20]. However, the cavity pocket formed by the flares behind the feed has a cross-shaped structure that is claimed to suppress unwanted higher-order modes. This antenna is slightly smaller than the proposed DRGH.

Very little information is available for the design presented in Ref. [19], and the simulated results were not validated with measurements of a prototype. Based on the available information, the antenna is smaller, comparable in size to the 1–18 GHz design presented in Ref. [12], and it does not have any E-plane sidewalls. The profile of the ridges is also similar to that in Ref. [12] with a constant ridge width. The coaxial-to-ridged waveguide launcher is mostly similar to traditional 1–18 GHz designs with flares [20]. The cavity pocket formed by the flares behind the feed is filled with a silicone magnetic absorber (ECCOSORB<sup>®</sup> FDS) similar to [16].

The design proposed in this paper is based on the 36:1 design in Ref. [31].

The design in Ref. [30] also uses a 2.4 mm connector to enable operation up to 50 GHz. Very few dimensions are given, but from Figure 3 in Ref. [30], it can be inferred that the antenna is significantly larger than the proposed DRGH. It does not have any E-plane sidewalls and includes a dielectric Luneburg lens. The ridges of the antenna have a constant ridge width and a ridge profile defined using Bezier curves, similar to [20]. The ridge gap is significantly larger. The coaxial-to-ridged waveguide launcher is mostly similar to traditional 1–18 GHz designs with flares [20]. However, perforations are made on all the sides of the launcher, and a magnetic silicone absorber (ECCOSORB<sup>®</sup> GDS) with a thickness of 0.76 mm is placed on top of all the launcher parts. Effectively, the launcher parts just have an absorber coating, unlike the honeycomb absorber-filled box of the proposed DRGH. As mentioned, the antenna was not manufactured, and only simulated results are presented.

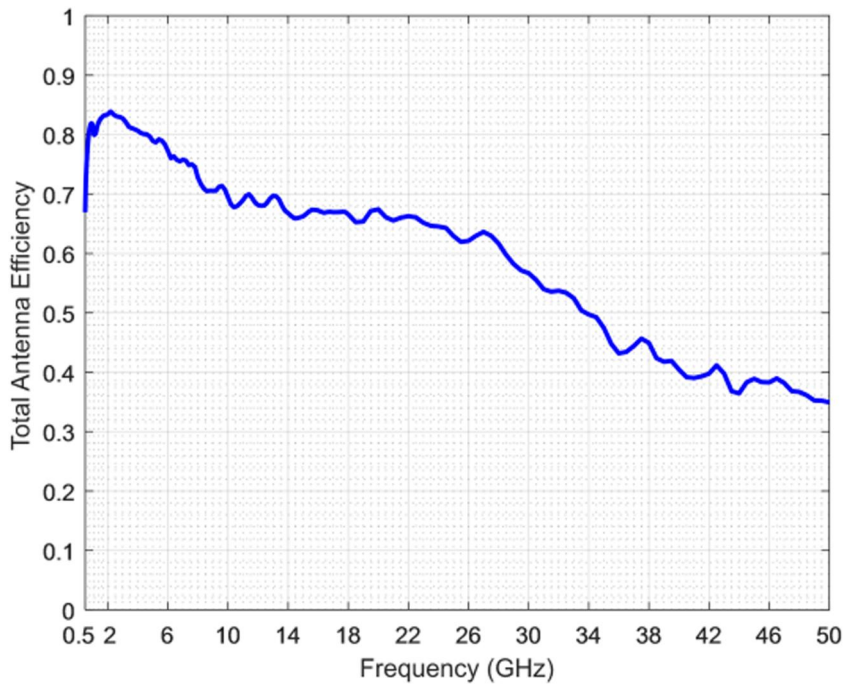


**FIGURE 22** Total antenna efficiency (simulated).

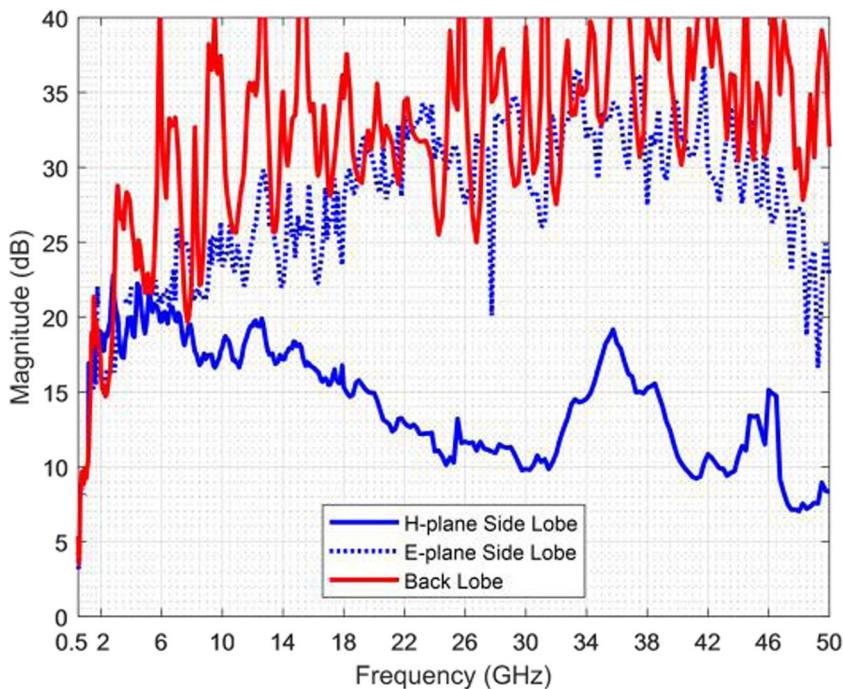


**FIGURE 23** Side and back lobe levels (measured).

In general, the DRGH radiation and VSWR performance above a certain frequency is dictated by the ridge design (around 2 GHz for the DRGH presented in this paper—as seen in Figures 7 and 16 as well as Figures 8 and 17). The ridge width, gap, and profile for the desired frequency range and performance can be found using parametric studies on the ridges in isolation. For higher frequency performance, the ridge

width and gap need to be reduced; for lower frequency performance, the ridge aperture and ridge axial length need to be increased. Inherently, the ridges in isolation are similar to the radiating portion of TEM and Vivaldi antennas and are nominally frequency-independent. The frequency of operation is only limited by practical manufacturing constraints, that is, the minimum sizes (ridge gap, width, and feed) that can be

**FIGURE 24** The position of the phase centre for the E- and H-plane patterns.

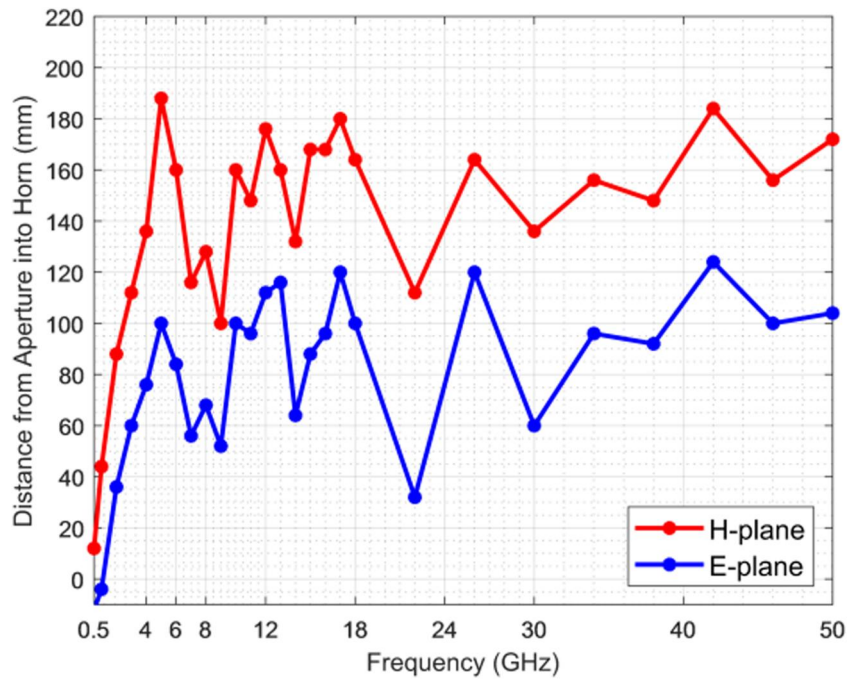
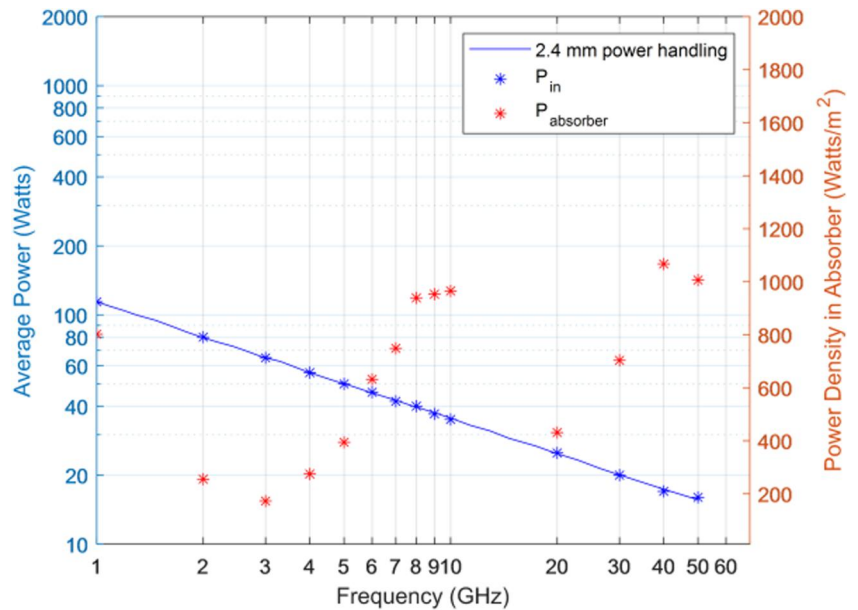


**FIGURE 25** Power density calculations in the absorber-filled cavity.



manufactured (high-frequency operation) and the maximum aperture and axial length of the flared section that can be accommodated (low-frequency performance).

As was discussed, the ridges need some connecting structure, typically in the form of a cavity which can take various forms, see Figures 2 and 5 in Ref. [31]. Introducing these cavities to the ridges breaks the nominal frequency-independent nature of the ridges. Over many years, changes and improvements in the cavity design, brought about mostly through experimentation using measurement and/or simulation, have resulted in increased DRGH bandwidth

performance. The problem is that if the cavity structure is too small, it will lead to the low-frequency end being below cut-off, and on the opposite end, if the cavity is too large, it will lead to high-frequency pattern breakup caused either by higher-order modes or reflection from the cavity walls.

Not all energy travels down the ridges and this causes backward radiation. At low frequencies, the backward radiation will be suppressed by the cavity structure; however, at high frequencies, the truncated structure of the ridges will still support backward radiation. This can be improved somewhat using a circular cavity similar to a Vivaldi antenna right behind the ridges,



**TABLE 3** DRGH bandwidth comparison.

Reference	Frequency range (GHz)	Bandwidth
[24]	2–40	20:1
[16, 17]	0.8–18	22.5:1
[27]	0.8–20	25:1
[19]	0.7–18	25.7:1
[31]	0.5–18	36:1
[30]	0.6–50	83:1
This work	0.5–50	100:1

but then there is still some radiation to the sides. The same problem is solved in cavity-backed spiral antennas using an absorptive cavity. It does result in the loss of some performance but allows significantly wider bandwidths compared to empty cavities. Another method would be to use a small cavity but fill it with lossy materials with high dielectric constant or magnetic permeability, for example, ferrites. Filling the cavity with material effectively increases the electrical size of the cavity for the low frequencies, and the lossy material will also reduce reflections and the excitation of modes at the high frequencies.

Adding flares and sidewalls to the DRGH improves low-frequency performance. For this antenna, the flares and sidewalls improve the performance between 1 and 2 GHz. Some high-frequency degradation is caused due to reflection from sidewalls, which necessitates the use of thin sidewall strips, but it is believed that an improved ridge design could reduce this effect.

## 6 | CONCLUSION

A single wideband DRGH antenna that can be used (as a source and reference) to measure 0.5–50 GHz antennas and systems was designed and implemented using additive manufacturing. A parametric study was performed to identify critical parameters in the design of the DRGH antenna for a bandwidth ratio of 100:1. To achieve such a wide bandwidth, the ridge gap, width, and feed were optimised, and a novel coaxial-to-ridge waveguide launcher section based on a typical Vivaldi antenna was developed. The addition of a sub-ridge and several tapered ridge width sections in the main ridge further improved the performance. Backward radiation and pattern breakup at mm-wave frequencies were reduced using an absorber-filled cavity and adding additional absorbers on cavity edges as well as carbon paint on the grid sidewalls. A mechanical design was performed based on the electrical model, and a prototype was manufactured. The prototype DRGH antenna achieved acceptable measured performance which compared well to simulated results.

This paper shows that it is possible to design DRGH antennas with bandwidth ratios of 100:1 and possibly beyond. It is believed that at higher frequencies, the limit will be the manufacturing tolerances and technology, and at the lower frequencies, the maximum permissible size of the antenna.

## AUTHOR CONTRIBUTIONS

**Bennie Jacobs:** Conceptualisation; Data curation; Formal analysis; Funding acquisition; Investigation; Methodology; Validation; Visualisation; Writing – original draft. **Johann W. Odendaal:** Funding acquisition; Supervision; Writing – review & editing. **Johan Joubert:** Funding acquisition; Supervision; Writing – review & editing.

## ACKNOWLEDGEMENTS

The authors would like to thank Saab Grintek Defence for their financial assistance and the use of their anechoic chambers and production facilities. Thanks also go to Dave Bullock from Rapid 3D (<https://rapid3d.co.za/>) for their assistance in the manufacture of the metal 3D printed feed section of the prototype antenna. SAAB Grintek Defence funded the manufacturing of the prototype antenna.

## CONFLICT OF INTEREST STATEMENT

No conflict of interest.

## DATA AVAILABILITY STATEMENT

The data that support the findings of this study are available from the corresponding author upon reasonable request.

## PERMISSION TO REPRODUCE MATERIALS FROM OTHER SOURCES

None.

## ORCID

Johann W. Odendaal  <https://orcid.org/0000-0002-5481-3723>

Johan Joubert  <https://orcid.org/0000-0003-2701-3947>

## REFERENCES

- NR: User equipment (UE) radio transmission and reception; Part 1: Range 1 Standalone. 3GPP TS 38, 101. V18.1.0, 2023-03, (2023)
- Cohn, S.B.: Properties of ridge waveguide. *Proc. IRE* 35(8), 783–788 (1947). <https://doi.org/10.1109/jrproc.1947.226277>
- Hopfer, S.: The design of ridged waveguides. *IRE Trans. Microw. Theor. Tech.* 3(5), 20–29 (1955). <https://doi.org/10.1109/tmtt.1955.1124972>
- Radio Research Laboratory Harvard University: Very High Frequency Techniques, pp. 725–728. McGraw-Hill, New York (1947)
- Walton, K.L., Sundberg, V.C.: Broadband ridged horn design. *Microw. J.*, 96–101 (1964)
- Kerr, J.L.: A very broad band low silhouette antenna. *Tech. Rep. ECOM-3087*. USAECOM, Fort Monmouth (1967)
- Kerr, J.L.: Broadband horns. *Tech. Rep. ECOM-3319*. USAECOM, Fort Monmouth (1970)
- Kerr, J.L.: Short axial length broad-band horns. *IEEE Trans. Antennas Propag.* 21(5), 710–714 (1973). <https://doi.org/10.1109/tap.1973.1140561>
- Bruns, C., Leuchtmann, P., Vahldieck, R.: Full wave analysis and experimental verification of a broad band ridged horn antenna system with parabolic reflector. In: *IEEE Antennas and Propagation Society International Symposium*, vol. 4, pp. 230–233. Boston (2001)
- Bruns, C., Leuchtmann, P., Vahldieck, R.: Analysis and simulation of a 1–18 GHz broadband double-ridged horn antenna. *IEEE Trans. Electromagn. Compat.* 45(1), 55–60 (2003)
- Bruns, C., Leuchtmann, P., Vahldieck, R.: Comprehensive analysis and simulation of a 1–18 GHz broadband parabolic reflector horn antenna

- system. *IEEE Trans. Antennas Propag.* 51(6), 1418–1422 (2003). <https://doi.org/10.1109/tap.2003.812236>
12. Rodríguez, V.: New Broadband EMC Double-Ridged Guide Horn Antenna, pp. 44–47. *RF Design* (2004)
  13. Rodríguez, V.: Dual ridge horn antenna. U. S. Patent 6 995 728 B2 (2006)
  14. Abbas-Azimi, M., et al.: Design and optimization of a new 1–18 GHz double ridged guide horn antenna. *J. Electromagn. Waves Appl.* 21(4), 501–516 (2007). <https://doi.org/10.1163/156939307780616810>
  15. Xu, H., et al.: Design and simulation of ultra-wideband double-ridged horn antenna. In: 2010 International Conference on Microwave and Millimeter Wave Technology, pp. 950–952. Chengdu, China (2010)
  16. Steghafner, H., Leugner, D., Klos, B. “Horn Antenna” U.S. Patent 7 969 376 B2 (2011)
  17. Rohde & Schwarz: “R&S HF907 Double-Ridged Waveguide Horn Antenna,” HF907 Datasheet, HF – VHF/UHF Antennas, Catalog (2017/2018)
  18. Ghorbani, M., Khaleghi, A.: Wideband double ridged horn antenna: Pattern analysis and improvement. In: Proceedings of the 5th European Conference on Antennas and Propagation (EUCAP), pp. 865–868. Rome (2011)
  19. Ghorbani, M.A., Khaleghi, A.: Double Ridged Horn Antenna Designs for Wideband Applications. In: 19th Iranian Conference on Electrical Engineering, pp. 1–4. Tehran (2011)
  20. Jacobs, B., Odendaal, J.W., Joubert, J.: An improved design for a 1–18 GHz double ridged guide horn antenna. *IEEE Trans. Antennas Propag.* 60(9), 4110–4118 (2012). <https://doi.org/10.1109/tap.2012.2207043>
  21. Abbas-Azimi, M., Arazm, F., Rashed-Mohassel, J.: Sensitivity analysis of a 1 to 18 GHz broadband DRGH antenna. In: *IEEE Antennas and Propag. Soc. Int. Symp.*, pp. 3129–3132. Albuquerque. (2006)
  22. Jacobs, B., Odendaal, J.W., Joubert, J.: The effect of manufacturing and assembling tolerances on the performance of double-ridged horn antennas. *J. Electromagn. Waves Appl.* 24(10), 1279–1290 (2010). <https://doi.org/10.1163/156939310791958761>
  23. Rodríguez, V.: Recent improvements to dual ridge waveguide horn antennas: The 200 MHz to 2000 MHz and 18 GHz to 40 GHz models. In: *IEEE International Symposium on Electromagnetic Compatibility*, pp. 24–27. Austin. (2009)
  24. Tenigeer, et al.: Design of a novel broadband EMC double ridged guide horn antenna. *PIER C* 39, 225–236 (2013). <https://doi.org/10.2528/pierc13032803>
  25. Morgan, M.A., Boyd, T.A.: A 10–100 GHz double-ridged horn antenna and coax launcher. *IEEE Trans. Antennas Propag.* 63(8), 3417–3422 (2015). <https://doi.org/10.1109/tap.2015.2439697>
  26. Wei, L., XiaoLi, X.: Design and simulation of TEM double ridge guide horn antenna. In: 8th International Conference on Electronic Measurement and Instruments pp. 70–3706, China (2007)
  27. Wang, C., et al.: Ridged horn antenna with adjustable metallic grid sidewalls and cross-shaped back cavity. *IEEE Antennas Wireless Propag. Lett.* 15, 1221–1225 (2016). <https://doi.org/10.1109/lawp.2015.2502578>
  28. Gerber, M., Odendaal, J.W., Joubert, J.: Ridge profile optimization of DRGH antenna. In: *IEEE Radio and Antenna Days of the Indian Ocean (RADIO)*, pp. 1–3. Mauritius (2018)
  29. Gerber, M., Odendaal, J.W., Joubert, J.: DRGH antenna with improved gain and beamwidth performance. *IEEE Trans. Antennas Propag.* 68(5), 4060–4065 (2020). <https://doi.org/10.1109/tap.2019.2948655>
  30. Kuroptev, P.D., Levyakov, V.V., Fateev, A.V.: Modified 0.6–50 GHz ultra-wideband double-ridged horn antenna design for parameters improvement. In: 47th European Microwave Conference (EuMC), pp. 465–468. Nuremberg (2017)
  31. Jacobs, B., Odendaal, J.W., Joubert, J.: “Compact 0.5–18 GHz double-ridged guide horn antenna,” *IET Microwaves. Antennas & Propag* 15(4), 427–440 (2021). <https://doi.org/10.1049/mia2.12058>
  32. Altair: “FEKO - Hyperworks, 2021 Release,” [altairhyperworks.com](http://altairhyperworks.com)
  33. Southwest Microwave “Power rating for coaxial connectors,” [Online]. <https://mpd.southwestmicrowave.com/wp-content/uploads/2020/09/Southwest-Microwave-Power-Rating.pdf>
  34. Fumeaux, C., Baumann, D., Vahldieck, R.: Finite-volume time-domain analysis of a cavity-backed Archimedean spiral antenna. *IEEE Trans. Antennas Propag.* 54(3), 844–851 (2006). <https://doi.org/10.1109/tap.2006.869935>
  35. ETS-Lindgren: “HP high power Microwave absorber,” datasheet, [Online]. <https://www.ets-lindgren.com/datasheet/absorbers/rf-absorbers/1006/100603>
  36. Cumming Microwave, “C-RAM SFC-HC high power broadbanded pyramidal honeycomb RF absorber,” Technical Bulletin 390-1, [Online]. <http://www.cummingmicrowave.com/wp-content/uploads/2013/06/390-16-C-RAM-SFC-HC.pdf>
  37. Microwave Vision Group: “HPX Series High Power Absorbers,” datasheet, [Online]. <https://www.mvg-world.com/media/1063/download/reference>
  38. Liu, L., et al.: Gradient honeycomb absorber with high power handling capability. *Appl. Phys. A.* 127(129), (2021). <https://doi.org/10.1007/s00339-020-04223-9>
  39. Zhang, Y., et al.: High-power broadband honeycomb absorber for 5G millimeter wave chambers. In: 2018 IEEE International Symposium on Electromagnetic Compatibility and 2018 IEEE Asia-Pacific Symposium on Electromagnetic Compatibility (EMC/APEMC), pp. 103–105. Suntec City, Singapore (2018)

**How to cite this article:** Jacobs, B., Odendaal, J.W., Joubert, J.: Wideband 0.5–50 GHz double-ridged guide horn antenna using coaxial-to-ridge waveguide launcher. *IET Microw. Antennas Propag.* 18(4), 248–265 (2024). <https://doi.org/10.1049/mia2.12441>